| | |
|---|---|
| $f_k(K)$ | complex scattering factor of whole of $k$th ion |
| $f_{sk}(K)$ | scattering factor of shell of $k$th ion |
| $-W_k$ | Debye–Waller exponent $= -B_k \sin^2\theta/\lambda^2$ |
| $\mathscr{E}(k/\mathbf{q}j)$ | orthonormalized eigenvector for ion $k$ in mode $(\mathbf{q}j)$ |
| $\mathscr{W}(k/\mathbf{q}j)$ | relative shell–core displacement eigenvector for ion $k$ in mode $(\mathbf{q}j)$ |
| $\mathbf{G}$ | a reciprocal-lattice vector |
| $\mathbf{r}(k)$ | equilibrium position of $k$th ion relative to origin of unit cell. |

### References


BORN, M. (1942). *Rep. Prog. Phys.* **9**, 294–333.

COCHRAN, W. & COWLEY, R. A. (1967). *Handbuch der Physik* XXV/29, pp. 59–156. Berlin: Springer.

DAWSON, B. (1964). *Acta Cryst.* **17**, 997–1009.

DOLLING, G. & WAUGH, J. L. T. (1965). *Lattice Dynamics*, edited by R. F. WALLIS, pp 19–32. Oxford: Pergamon.

*International Tables for X-ray Crystallography* (1974). Vol. IV. Birmingham: Kynoch Press. (Present distributor D. Reidel, Dordrecht.)

KUNC, K. & NIELSEN, O. H. (1979). *Comput. Phys. Commun.* **17**, 413–422.

MARCH, N. H. & WILKINS, S. W. (1978). *Acta Cryst.* A**34**, 19–26.

MATTHEW, J. A. D. & YOUSIF, S. Y. (1984). *Acta Cryst.* A**40**, 716–721.

MELVIN, J. S., PIRIE, J. D. & SMITH, T. (1968). *Phys. Rev.* **175**, 1082–1090.

PRICE, D. L., ROWE, J. M. & NICKLOW, R. M. (1971). *Phys. Rev. B*, **3**, 1268–1279.

REID, J. S. (1974). *Phys. Status Solidi B*, **64**, 57–64.

REID, J. S. (1983*a*). *Acta Cryst.* A**39**, 1–13.

REID, J. S. (1983*b*). *Acta Cryst.* A**39**, 533–538.

SCHUSTER, S. L. & WEYMOUTH J. W. (1971). *Phys. Rev. B*, **3**, 4143–4153.


*Acta Cryst.* (1987). A**43**, 102–112

# Problems Associated with the Measurement of X-ray Attenuation Coefficients. I. Silicon

## Report on the International Union of Crystallography X-ray Attenuation Project


BY D. C. CREAGH*

*Physics Department, Royal Military College, Duntroon, ACT* 2600, *Australia*

AND J. H. HUBBELL

*Center for Radiation Research, National Bureau of Standards, Gaithersburg, MD* 20899, *USA*


(*Received* 20 *October* 1985; *accepted* 17 *July* 1986)


### Abstract

X-ray attenuation coefficient measurements made on single-crystal silicon specimens by participants in the International Union of Crystallography X-ray Attenuation Project are presented for the energy range 8–60 keV. Twelve laboratories using eight different experimental configurations have provided data for analysis. A comparison is made between measurements using the different techniques at those characteristic wavelengths of interest to crystallographers. Comparison of these measurements with available theoretical cross sections suggests that a model in which the thermal diffuse scattering cross section is used instead of the Rayleigh scattering cross section for the calculation of the theoretical total scattering cross section gives better agreement with the experimental values. No basis was found for preferring one of three current theoretical tabulations of photoelectric absorption cross section over the others.


* Present address: Physics Department, University College, Australian Defence Force, Campbell, ACT 2600, Australia.

## 1. Introduction

### 1.1. *Tables of X-ray attenuation coefficients*

Following the discovery by Röntgen (1895) of the penetrating nature of X-rays, a considerable body of numerical data concerning the attenuation of X-rays by matter has accumulated in the scientific literature. The earliest quantitative measurements of X-ray attenuation coefficients appear to be those by Barkla & Sadler (1907), after which researchers in a wide variety of disciplines (*e.g.* X-ray crystallography, atomic physics, medical diagnosis and therapy, electron probe microanalysis) contributed data sets which form the basis of such widely circulated compilations as those by McMaster, Del Grande, Mallett & Hubbell (1969) and by Storm & Israel (1970). The McMaster *et al.* (1969) compilation includes a list of data sources and a confidence weight assigned to each data-source document. A data index to these data sources through 1971 was given by Hubbell (1971).

Many other compilations exist [*e.g.* Allen (1935, 1969); Victoreen (1949); Liebhafsky, Pfeiffer, Win-

0108-7673/87/010102-11$01.50 

slow & Zemany (1960); Koch, MacGillavry & Milledge (1962); Heinrich (1966); Theisen & Vollath (1967); Veigele (1973); Leroux & Thinh (1977); Montenegro, Baptista & Duarte (1978); Plechaty, Cullen & Howerton (1981); Henke, Lee, Tanaka, Shimabukuro & Fujikawa (1982)], and if one seeks to compare them, one often finds significant discrepancies between entries. The question then arises as to which of the tables contains the more reliable data, or, at least, what is a realistic envelope of uncertainty.

The substantial uncertainties in present compilations, resulting from these discrepancies in the experimental database, are unacceptable to researchers in a wide variety of fields. The extensive use of X-ray fluorescence and electron microprobe analysis by metallurgists and mineralogists for quantitative determinations of composition has created a need for better data sets for the X-ray attenuation coefficients. In addition, health physicists need to have accurate data for those elements which are the principal constituents of plant and animal tissue, but such data are not available to a desirable high precision. For medical diagnosis using X-ray techniques, the advent of computer-aided tomography (CAT) has increased the demand for accurate data, and Jackson & Hawkes (1981) have recently produced a set of parametric fits for the individual collision processes intended for use in quantitative CAT-scan applications.

In almost every aspect of experiments involving X-ray diffraction the interpretation of the raw data requires a knowledge of the relevant X-ray attenuation coefficients before meaningful results can be obtained. We thus offer some general comments on the tables of X-ray attenuation coefficients and the manner in which they are generated and used.

Some tables are based entirely on theoretical calculations. For example, one tabulation of the photoelectric absorption cross section for X-rays was computed by Cromer & Liberman (1970) using a program developed by Brysk & Zerby (1968). Energy eigenvalues, however, were not computed. Rather, the experimental values of Bearden & Burr (1967) were used. Among the other theoretical photoabsorption tables in the region of interest to crystallographers are those of Hildebrandt, Stephenson & Wagenfeld (1975) using hydrogen-like eigenfunctions and providing dipole and quadrupole cross-section components for Borrmann-effect applications. Band, Kharitonov & Trzhaskovskaya (1979) have also computed tables of photoabsorption cross sections, using relativistic self-consistent Dirac–Slater potentials and including parametrized photoelectron angular distribution information.

Tabulations also exist for the Compton (modified) scattering cross section (Hubbell, Veigele, Briggs, Brown, Cromer & Howerton, 1975) and for the Rayleigh (unmodified) scattering cross section (Hubbell & Øverbø, 1979; Schaupp, Schumacher, Smend, Rullhusen & Hubbell, 1983).

It is usually assumed that the overall photon attenuation cross section of an atom is the sum of the contributions from photoelectric absorption and the Compton and Rayleigh scattering cross sections. It is further assumed that, for an assemblage of atoms, the individual atomic cross sections are summed to determine the total X-ray attenuation coefficient.

This simple additivity rule, some limitations of which have been discussed by Deslattes (1969), is central to all uses of the tables as a means for estimating X-ray attenuation coefficients. It follows, therefore, that any meaningful technique for measuring X-ray attenuation coefficients should measure only the absorption and scattering of X-rays by atoms and minimize the effect of cooperative scattering by regular arrays of atoms.

Tabulations on experimental data, such as that of McMaster *et al.* (1969, 1970) make judgements on the reliability of data based on the type of experiment used and the reputation of the experimentalist involved. A table is then built up by mathematical interpolation, with some guidance from available theory, between the experimental data points. Tabulations of this kind are likely to include data for which a wide variety of cooperative processes are involved, and consequent systematic errors ensue when these cross sections are combined using the additivity rule.

### 1.2. *The International Union of Crystallography X-ray Attenuation Project*

It is of some importance to identify those experimental techniques which are likely to minimize systematic error. The Commission for Crystallographic Apparatus of the International Union of Crystallography (IUCr) recognized the need for such an examination of existing techniques, and in 1979 at the Eleventh General Assembly, Warsaw, inaugurated a project to attempt to resolve the problem.

Although there would be some value in measuring and remeasuring X-ray attenuation coefficients for all elements in crystalline, amorphous and other physical states, and also in molecular and ionic compounds, for all wavelengths (or photon energies) of conceivable IUCr interest, we have limited the project, initially, at least, to the following aims:

(1) to establish which techniques for the measurement of X-ray attenuation coefficients give rise to the most reliable data;

(2) to compare the data so obtained with the tabulated values;

(3) to establish which of the tabulations are to be considered as reliable, and to what extent they may be considered to be reliable.

The procedure for achieving the primary aim was as follows. Sets of standard materials were prepared

and were intended to be representative of classes of materials which might be encountered in practice. They comprised: slices of highly pure single-crystal silicon; pieces of pyrolytic graphite; and discs punched from highly rolled strips of copper. On joining the project a participant was sent a set of specimens and was asked to use whatever technique he considered to be most appropriate for the measurement of X-ray attenuation coefficients for each class of material. Twelve laboratories, using eight different experimental configurations, have so far returned data to be included in the project's files.

This paper will consider the results obtained for silicon. Later papers will deal in turn with the results for graphite and copper.

## 2. Theory

### 2.1. *Definitions*

The X-ray attenuation coefficients referred to in the introduction are those which result when a narrow beam of monochromatic X-rays passes through a plane parallel layer of homogeneous material which has surfaces normal to the beam direction and broad compared with the beam cross section. The Beer–Lambert law then applies and

$$I = I_0 \exp(-\mu_l x), \tag{1}$$

where $I_0$ is the intensity of the incident beam and $I$ is the intensity of the emergent beam. The directions of the incident and emergent beams must be exactly the same. The path length of the beam in the material is $x$.

The linear attenuation coefficient of the material is $\mu_l$, which is dependent on the sample density, in addition to the effective atomic weight and atomic-structure properties of the sample. Hence, since the density of a given elemental substance can vary widely (allotropic *versus* various crystalline forms, vapor/liquid/solid phases, thermal expansion *etc.*), a coefficient more uniquely characterizing a given substance is the density-independent *mass attenuation coefficient* $\mu_m$ widely used in general-purpose X-ray attenuation data compilations.

The mass attenuation coefficient is defined as

$$\mu_m = \mu_l / \rho \tag{2}$$

where $\rho$ is the density of the medium.

The mass attenuation coefficient is proportional to the total photon interaction cross section per atom,

$$\sigma = \mu_m M / N_A, \tag{3}$$

where $N_A$ is the Avogadro number and $M$ is the atomic weight of the sample material.

For the X-ray energy range considered here (photon energies less than 1·02 MeV, the pair-production threshold) the total photon interaction cross section is given by

$$\sigma = \sigma_{\text{pe}} + \sigma_{\text{modified}} + \sigma_{\text{unmodified}}. \tag{4}$$

The cross sections $\sigma_{\text{pe}}$, $\sigma_{\text{modified}}$, and $\sigma_{\text{unmodified}}$ will be discussed in the following sections.

### 2.2. *The photoelectric absorption cross section* $\sigma_{pe}$

Relativistic quantum mechanics is used by many authors in their calculation of $\sigma_{\text{pe}}$. The photoelectric cross section is given by

$$\sigma(\hbar\omega) = (4\pi^2 e^2 m/\omega c) mc^2 \times |\langle \varepsilon_1 + \hbar\omega | \mathbf{l} \,.\, \boldsymbol{\alpha} \exp(i\mathbf{k} \,.\, \mathbf{r}) | \rangle|^2 \tag{5}$$

where $\hbar$, $\omega$, $e$, $c$ have their usual meanings; 1 represents the initial state wavefunction for the electron, and $\varepsilon_1 + \hbar\omega$ represents its final state wavefunction; $\mathbf{l}$ is the polarization vector for the photon; $c\boldsymbol{\alpha}$ is the Dirac velocity operator; and $\exp(i\mathbf{k} \,.\, \mathbf{r})$ represents the wave being scattered by the electron.

Treatments differ somewhat in the type of potential used to compute the electron wavefunctions and the choice of energy eigenvalues to be used in the computation of the Dirac–Slater eigenvalues.

The result is that several sets of tables exist and differences between tables arise because of the manner in which the Dirac–Slater eigenvalues are computed.

The approach used by Scofield (1973) employs Hartree–Slater wavefunctions and uses a different exchange potential from the other workers cited earlier. The recent tabulation by Hubbell (1982) uses Scofield's data modified for $Z = 1$ to 54 using relativistic Hartree–Fock renormalization factors supplied by Scofield (1973).

In general the theoretical data sets for $\sigma_{\text{pe}}$ agree well with one another, although the Scofield data tend to be systematically higher than those of Cromer & Liberman (1970) and Storm & Israel (1970). It must be remembered, however, that these other two have a common origin in the Brysk & Zerby (1968) computer program.

### 2.3. *Incoherent (Compton) scattering,* $\sigma_C$

The bound-electron Compton scattering cross section is given [see, for example, Hubbell (1969)] by the relation

$$\sigma_C = \pi r_e^2 \int_{-1}^{1} [1 + k(1 - \cos\varphi)]^{-2} \times \{1 + \cos^2\varphi + k^2(1 - \cos\varphi)^2 \times [1 + k(1 - \cos\varphi)]^{-1}\} I(s) \mathrm{d}(\cos\varphi), \tag{6}$$

where $r_e$ is the classical radius for the electron; $k = \hbar\omega/mc^2$, the photon energy in units of electron rest mass; $\varphi = 2\theta$, the angle between incident and scattered photon directions, where $\theta$ is the Bragg angle;

$s = \sin\theta/\lambda$; and $I(s)$ = incoherent intensity expressed in electron units.

The incoherent intensity $I(s)$ used for the calculation of $\sigma_C$ in §4 was that of Cromer & Mann (1967) and Cromer (1969).

### 2.4. *Unmodified scattering*

2.4.1. *Rayleigh scattering, $\sigma_R$.* If each of the atoms giving rise to unmodified scattering can be considered to scatter as though it were an isolated atom, the cross section can be written as

$$\sigma_R = 2\pi r_e^2 \int_{-1}^{1} C_p f^2(s)\, \mathrm{d}(\cos\varphi), \tag{7}$$

where $C_p = \frac{1}{2}(1+\cos^2 2\theta)$; $s = \sin\theta/\lambda$; and $f(s)$ is the atomic scattering factor or atomic form factor.

Tables of $f(s)$ and $\sigma_R$ have been published recently by Hubbell & Øverbø (1979) and of $f(s)$ by Schaupp *et al.* (1983).

2.4.2. *Laue–Bragg scattering, $\sigma_{LB}$.* If the atoms are arranged on a crystal lattice another type of unmodified scattering can take place. This is referred to as Laue–Bragg scattering.

For a finely divided crystalline powder one can write, for the total power $P_H$ scattered in a Debye–Scherrer cone,

$$P_H = m_H I_0 Q_H \delta_V \tag{8}$$

where $m_H$ is the multiplicity of the Bragg reflection; $I_0$ is the incident beam intensity; $Q_H = (r_e/V_c)^2 C_p |F_H|^2 \lambda^3/4\sin\theta$; $\delta_V$ is the volume of the crystalline particle; $V_c$ is the volume of the unit cell; $F_H$ is the geometrical structure factor for the reflection having Miller indices $h$, $k$, $l$. $Q_H$ is the attenuation factor, since it represents the ratio of scattered to incident power.

The total scattering cross section is found by summing over all possible $h$, $k$, $l$ reflections. For a crystal having $N$ atoms per unit cell,

$$\sigma_{LB} = (r_e^2\lambda^2/2NV_c) \sum_H [C_p m d |F|^2 \exp(-2M)]_H. \tag{9}$$

Here $d_H$ is the spacing of the $(hkl)$ planes and has arisen because the Bragg equation was used to eliminate the $\sin\theta$ term. The temperature factor $\exp(-2M)$ has also been determined from the geometrical structure factor. The approach outlined above is due to de Marco & Suortti (1971). Other similar calculations have been made by Gerward, Thuesen, Stibius Jensen & Alstrup (1979).

In this approach the assumption of cooperative scattering implies that a further scattering mechanism exists: that of thermal diffuse scattering.

2.4.3. *Thermal diffuse scattering, $\sigma_{TD}$.* It is assumed that the total thermal diffuse scattering is equal to the scattering lost from Laue–Bragg scattering because of thermal vibrations:

$$\sigma_{TD} = (r_e^2\lambda^2/2NV_c) \sum_H \{C_p m d |F|^2 [1-\exp(-2M)]\}_H. \tag{10}$$

this is not in a very convenient form for analysis and an alternative formalism presented by Sano, Ohtaka & Ohtsuki (1969) has been used in calculations. In this formalism

$$\sigma_{TD} = 2\pi r_e^2 \int_{-1}^{1} C_p f^2(s) \times \{1-\exp[-2M(s)]\}\, \mathrm{d}(\cos\varphi). \tag{11}$$

Values of $f(s)$ have been tabulated by Cromer & Waber (1965).

The cross section tends to oscillate in the low-energy range and this corresponds to the inclusion of new Bragg peaks in the summation. Eventually the oscillations damp down and $\sigma_{TD}$ becomes a smoothly varying function of energy.

### 2.5. *The total cross section*

In forming an expression for the total cross section it is necessary to make some assumption as to the extent to which cooperative unmodified scattering might take place. Whether one uses

$$\sigma = \sigma_{pe} + \sigma_C + \sigma_R \tag{12}$$

or

$$\sigma = \sigma_{pe} + \sigma_C + \sigma_{LB} + \sigma_{TD} \tag{13}$$

can be of some significance when attempting to reconcile theoretical calculations and experimental measurements.

The choice of specimens distributed to the participants in this project was influenced by this fact. In this and later papers the influence which cooperative scattering has on the observed and calculated total cross section will be examined.

## 3. Experimental techniques

### 3.1. *Specimen preparation*

Two sets of silicon specimens were prepared. One set was cut from a cylindrical boule of high-purity electron-beam float-zoned single-crystal silicon, the cylinder axis of which lay parallel to [220]. The other set was cut from a cylindrical boule of similar purity but which had the cylinder axis parallel to [111]. The samples had, typically, a surface area 15 × 15 mm and thickness varying from 0·4 to 4 mm, chosen to enable the Nordfors (1960) criterion for optimum counting statistics to be fulfilled by either one specimen or a combination of specimens for wavelengths commonly used by crystallographers.

From the boule having [111] orientation a similar range of specimen blocks was prepared. The orienta-

tion of the normal to the (15×15 mm) surfaces was set to be within 0·25° of the [111].

### 3.2. *Characterization of specimen sets*

Sets of specimens each containing seven blocks of silicon were distributed to participants in the project. For each component of each set the following data were taken: (i) the surface dimensions (measured to an accuracy of 0·01 mm using an optical comparator); (ii) its nominal thickness; (iii) its mass (measured on a digital balance accurate to $10^{-9}$ kg).

The density of the silicon was determined using the technique described by Henins (1964). The average densities of both the [220] and the [111] oriented silicon blocks were observed to be the same, corresponding to a value of 2·3300(2) g cm$^{-3}$ at 293 K. The value determined by Henins was 2·3290002(7) g cm$^{-3}$ at 298 K [or 2·3290875 g cm$^{-3}$ at 293 K, assuming a coefficient of linear thermal expansion of 2·5×$10^{-6}$ as given by Kirby, Hahn & Rothrock (1972)]. These two results are in excellent agreement with one another.

In addition, at least one speciment from each set, usually the thinnest, was tested for gross mechanical damage and plastic deformation using diffracted-beam X-ray topography (Lang, 1958). Also any significant tapering and other variations in thickness show up as *Pendellösung* fringes in the X-ray topographs.

### 3.3. *Experimental configurations*

A survey of the techniques used for the measurement of X-ray attenuation coefficients for the period 1895 to 1983 showed that, for all of the experiments reported in that period, one quarter had an incident beam which may have had second-harmonic contamination, one third made no dead-time corrections and one third described configurations with excessive (by modern standards) beam divergence.

It is not surprising, therefore, that systematic errors are present in tables which are based on experimental data.

A schematic representation of the configurations employed by members of the project is shown in Fig. 1. It is not the intention here to describe in detail the performance of each component in these configurations. Reference to standard texts on X-ray diffraction and X-ray fluorescence spectrometry (*e.g.* Klug & Alexander, 1973; Bertin, 1975) will make clear the limitations of each component.

Fig. 1(*a*) shows the simplest configuration (1) employed in the project. For this the source was a fine-focus X-ray diffraction tube, and monochromatization was effected by means of an appropriate $\beta$ filter. The source was operated at a voltage such that $\lambda/2$ radiation was not generated. The beam was formed by means of a collimator and slit system, the

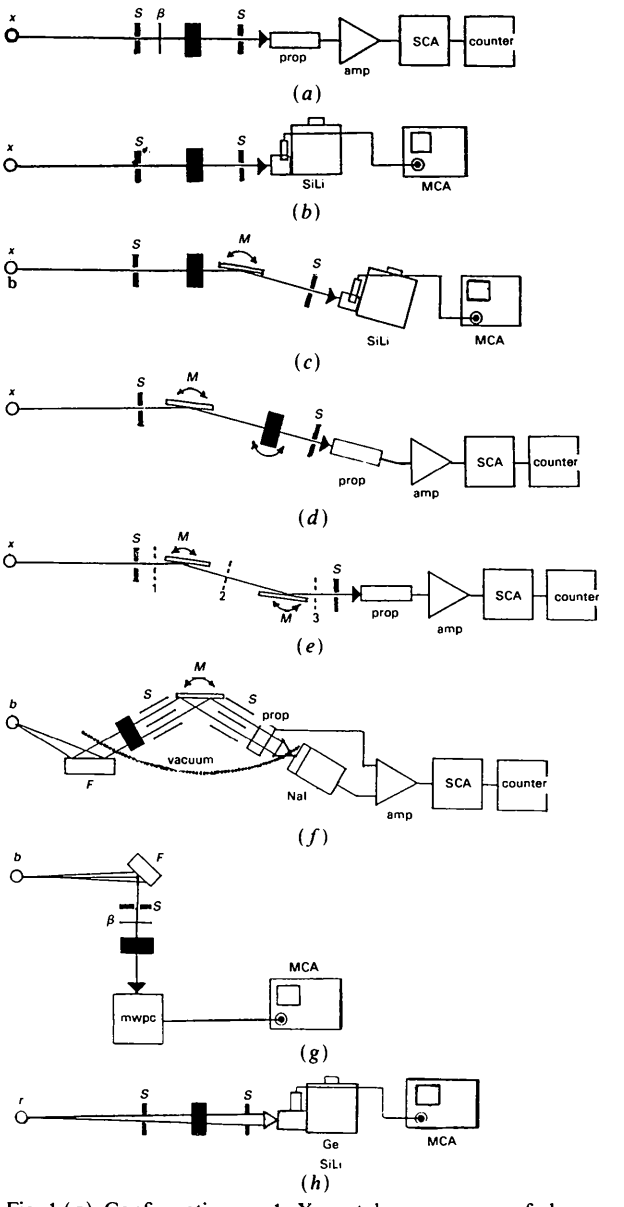


Fig. 1.(*a*) Configuration no. 1: X-ray tube as a source of characteristic radiation *x*, slits *S* before and after sample; monochromatizing by $\beta$ filter; energy discrimination by proportional counter, single-channel analyzer. (*b*) Configuration 2: same as (*a*) except monochromatizing by solid-state detector and multichannel analyzer. (*c*) Configuration 3: same as (*b*) except additional wavelength selection by crystal diffraction monochromator *M* between sample and second slit. (*d*) Configuration 4: same as (*c*) except crystal diffraction monochromator is between first slit and sample. (*e*) Configuration 5: double-crystal monochromator, with sample placed at any of the three positions (1, 2, 3) between the slits and monochromatizing crystals. (*f*) Configuration 6: X-ray *Bremsstrahlung* source *b* irradiating fluorescing target *F*, followed by the sample, then Soller slits before and after a single-crystal diffraction monochromator, then an energy-selective detector system. The sample, Soller slits, analyzing crystal and proportional detector are in a vacuum vessel. (*g*) Configuration 7: source is a fluorescing target, followed by a slit, filter and sample, then proportional counter. (*h*) Configuration 8: Same as (*b*) except X-ray tube is replaced by a radioactive source *r*.

angular divergence of the beam about 1 msr. The sample was mounted normal to the beam axis, and behind this was a coaxially mounted slit system, the aperture of which was kept fixed during the experiment. Following this was a proportional counter and single-channel analyzer, the latter enabling rough energy discrimination to be achieved. The relatively poor energy resolution ($\sim$30% at Cu $K\alpha_1$) makes the detection of any Compton scattered or X-ray fluorescence radiation from the sample or slit systems difficult.

The second configuration (no. 2) shown in Fig. 1(*b*) is similar to no. 1 except that the proportional detector is replaced by either an Si(Li) or an intrinsic germanium solid-state detector linked to a multichannel analyzer. Such detectors have good energy resolution ($\sim$2% at Cu $K\alpha_1$) and it becomes possible to recognize contaminating radiation in the transmitted beam. Furthermore it is possible to eliminate the filter and to use the *Bremsstrahlung* radiation from the target to irradiate the target, thus recording the attenuation at many wavelengths simultaneously.

The configuration shown in Fig. 1(*c*) utilizes a perfect silicon crystal (usually with its face cut parallel to [111]) to act as a monochromator for the transmitted radiation. Because a solid-state detector is employed, wavelengths from the *Bremsstrahlung* as well as characteristic lines may be used for measurements.

In Fig. 1(*d*) the monochromator is placed in front of, rather than behind, the specimen. Three variations of this configuration were used:

(i) a curved-crystal monochromator and a scintillation-counter detection system;

(ii) a germanium single crystal cut with its surface parallel to [111] and detection by means of a solid-state detector and multichannel analyzer;

(iii) a silicon monochromator and a proportional-counter system.

For (i) and (ii) the sample was mounted perpendicular to the beam. The third configuration differs from all the others used in the project in that the path length through the specimen is varied by rotating the specimen in the beam. This technique, described by Lawrence (1977), is often used in experiments for which only one thickness of specimen is available.

To ensure that the beam transmitted through the specimen has exactly the same wavelength as the incident beam one could place a second monochromator between the sample and the detector, as shown in Fig. 1(*e*). This double-crystal configuration has been widely used by Hildebrandt, Stephenson & Wagenfeld (1973). A more complicated device was described by Creagh (1978).

All the preceding techniques have used a sealed X-ray tube as the source of X-rays. An alternative method for the generation of X-rays employs X-ray-induced fluorescence to produce the desired X-ray wavelength. Fig. 1(*f*) shows a modification which can be made to a conventional XRF spectrometer to enable it to measure X-ray attenuation coefficients. In this case (no. 6) the specimen is mounted on a carrier inside the vacuum chamber between the fluorescing sample and the specimen. The limitations of a variation of this configuration, commonly used by XRF spectroscopists, in which the sample is placed outside the vacuum chamber between the crystal and the detector, have been discussed by Creagh (1976).

Configuration 7 (Fig. 1*g*) uses an X-ray fluorescence source and appropriate filtration to select the incident wavelength. Additional energy discrimination is provided by the use of a specially designed proportional counter.

The simplicity and ready availability of radioisotope sources make their use in equipment for the measurement of X-ray attenuation attractive. Systems which are used for these measurements are mechanically very simple (Fig. 1*h*), and energy discrimination is usually effected by the use of a solid-state detector and multichannel analyzer.

### 3.4. *Counting strategies*

3.4.1. *Choosing the specimen thickness.* It must be stressed that it is necessary to verify that the Beer–Lambert law is obeyed for the specimens under test. If a plot of $\ln(I_0/I)$ against thickness or mass per unit area does not yield a straight line then no unique X-ray attenuation coefficient exists and an investigation must take place to establish what is the cause of the nonlinearity.

If it is established that a unique value exists for $\mu_l$ or $\mu_m$, measurements can then be made at those specimen thicknesses for which the counting statistics can be optimized. Criteria for such a choice have been given by Nordfors (1960). Best results are obtained for those thicknesses which satisfy

$$2 \leq \ln(I_0/I) \leq 4. \qquad (14)$$

Appropriate dead-time corrections (*e.g.* Chipman, 1969) must be applied to the measurements of $I_0$ and $I$ before values for $\mu_l$ or $\mu_m$ are derived from the raw data. In all experiments the dead time should be determined experimentally. This is especially necessary for systems using multichannel analyzers because a significant component of instrumental dead time arises from the pulse-height analysis and storage processes. It is often wise to utilize the full capacity of the multichannel analyzer for energy analysis to establish which energy regions are of interest and then to use single-channel analyzers set to these energies to make the final measurements. All of the participants in the IUCr X-ray attenuation project used empirically determined dead-time corrections for the resolution of their data. Creagh used the single-channel analyzer technique for the measurements he made using solid-state detection systems.

Table 1. *Silicon linear attenuation coefficients at five selected photon energies, 8·048 to 59·57 keV, obtained by eight measurement techniques*

Also given are the McMaster *et al.* (1969, 1970) [basis for *International Tables for X-ray Crystallography* (1974) (IT IV)] values for comparison. Experimental errors are typically claimed to be ±1%.

| Radiation* | Wavelength (Å) | Energy (keV) | 1 | 2 | 3 | 4 | 5 | 6 | 7 | 8 | IT IV |
|---|---|---|---|---|---|---|---|---|---|---|---|
| Cu $K\alpha_1$ | 1·5405 | 8·048 | 146·2† | 145·6† | 146† | 142·5 | 144·2 | **144** | 144·9 | | 152 |
| | | | **145·8**† | **145**† | **144·6** | 142·2‡ | | 143·3 | | | |
| | | | | | 144·6† | | | | | | |
| Mo $K\alpha_1$ | 0·7092 | 17·487 | 14·66† | **14·62** | 14·63 | 14·51‡ | 14·68 | 144·72 | 14·60 | | 15·2 |
| | | | | 14·60† | 14·61 | | | **14·63** | | | |
| | | | | | 14·60† | | | | | | |
| | | | | | **14·60** | | | | | | |
| Ag $K\alpha_1$ | 0·5594 | 22·162 | **7·20**† | **7·20**† | **7·18** | 7·53 | | 7·24 | | | 7·55 |
| | | | | | 7·18 | 7·09‡ | | 7·16 | | | |
| | | | | | | | | **7·10** | | | |
| White | 0·3094 | 40·06 | | | **1·472** | | | | | | 1·57 |
| | | | | | 1·468‡ | | | | | | |
| $^{241}$Am | 0·2081 | 59·57 | | | | | | | | 0·742 | 0·740 |
| | | | | | | | | | | 0·739 | |

* Configurations 1, 2, 4, 6, 7 give measurements for $K\bar{\alpha}$ rather than $K\alpha_1$. The $K\alpha_1$ value shown here was derived using an interpolation procedure.
† Measurements on [111] oriented silicon. All other measurements were for [220] oriented silicon.
‡ Measurements with the technique involving tilting the specimen in the beam.

## 4. Results: silicon

### 4.1. *Selected experimental data*

Results have been received for photon energies ranging from 8 to 1173 keV. Table 1 presents selected data: data which may be of direct significance to an X-ray crystallographer. Data are tabulated for the characteristic $K\alpha_1$ radiations of copper, molybdenum and silver, a radiation wavelength selected from the *Bremsstrahlung*, and a $\gamma$-ray from $^{241}$Am. This table compares values of the linear attenuation coefficient $\mu_l$ which have been determined by the different experimental configurations described in § 3.3. Values shown in bold are measurements made by Creagh, using experimental configurations approximating those of a project participant.

Attention is drawn to those values denoted by the dagger(†) in Table 1. These data were obtained using Si specimens cut perpendicular to [111]. The other values were obtained using the [220] oriented samples. The effect of the Laue–Bragg scattering by these samples is less than by those having the [111] orientation.

To eliminate the problem with Laue–Bragg scattering, an extremely well collimated incident beam is required. For example, the measurements at Cu $K\alpha_1$ in columns 1 and 2 of Table 1 did not have good collimation whereas those in column 3 did. The difference between these sets of readings is comparable to the Laue–Bragg scattering value of $\sim 1{\cdot}7\ \text{cm}^{-1}$.

Low values of $\mu_l$ usually occur because of scattering into the beam of a Compton-scattered component or because of failure to account correctly for fluorescence background intensities. Such problems can occur in X-ray fluorescence spectrometers (no. 6) since these use broad Soller-slit collimated beams.

In no. 4 the monochromator is placed in front of the crystal. The two measurements were made in quite different fashions. In the first ($142{\cdot}5\ \text{cm}^{-1}$) the specimen was placed perpendicular to the beam diffracted by a curved monochromator and the transmitted beam was detected by a sodium iodide scintillation detector.

The lower value was found using the technique in which the specimen is placed at an angle to the beam diffracted by a flat [111] silicon single crystal. A proportional detector was used. It is probable that Compton in-scattering and slit fluorescence is the cause of error in these cases, since neither detection system has the capacity to detect their presence.

The most reliable data we consider to be those collected using configuration 3. Both Gerward (1981, 1982) and Creagh have independently investigated the influences on the value of $\mu_l$ of the rotation of the sample about its surface normal and the nature of dead-time corrections to be used when multichannel analysis is used. Both experiments yielded the same value for $\mu_l$ [$=144{\cdot}6(1)\ \text{cm}^{-1}$] although they were made on specimens having different orientations. This suggests that the influence of Laue–Bragg scatter has been minimized in both experiments.

Because we consider these two experiments to be the most carefully performed of the group, we propose the value of $144{\cdot}6(6)\ \text{cm}^{-1}$ as the 'present best' value for $\mu_l$.

The value derived from McMaster *et al.* (1969, 1970) is $152\ \text{cm}^{-1}$.

For Mo $K\alpha_1$, most of the experimental configurations yielded results which lay within 1% of the mean $14{\cdot}62\ \text{cm}^{-1}$. Evidently the difficulties with respect to Laue–Bragg scatter apparent in the Cu $K\alpha_1$ measurements are not significant for Mo $K\alpha_1$.

The technique in which the specimen is tilted has again yielded a low result, probably owing to Compton in-scattering from the specimen.

Note that there is now no significant difference between the results for [220]- and [111]-cut silicon, suggesting that Laue–Bragg scatter is unimportant at this photon energy.

The 'present best' value we propose for $\mu_l$ is 14·60(2) $cm^{-1}$, whereas the value taken from McMaster *et al.* (1969, 1970) is 15·2 $cm^{-1}$.

The results for Ag $K\alpha_1$ are generally in good agreement with one another, with one or two exceptions. It should be noted that the technique which involves tilting the specimen again yields a lower value than the other techniques.

Again the most reliable data have been acquired using configuration 3. We propose the value of 7·18(2) $cm^{-1}$ as the 'present best' value of $\mu_l$ at this wavelength.

Only two laboratories used a monochromator to select photon energies from the *Bremsstrahlung* continuum, and their results are in excellent agreement with one another. The technique used was no. 3. The results from one of these laboratories have recently been published (Mika, Martin & Barnea, 1985). The mean of 1·470(2) $cm^{-1}$ may be taken as the 'present best' value of $\mu_l$ at a photon energy of 40·06 keV. The value given by McMaster *et al.* (1969, 1970) is 1·57 $cm^{-1}$.

Two laboratories have returned data taken at 59·57 keV with a radioisotope source using configuration 8. At this photon energy Compton scattering and unmodified scattering processes become important and the problems associated with the crystalline nature of the specimen are largely irrelevant.

The mean value 0·740(2) $cm^{-1}$ is identical to the value of 0·740 $cm^{-1}$ interpolated from the values given in McMaster *et al.* (1969, 1970).

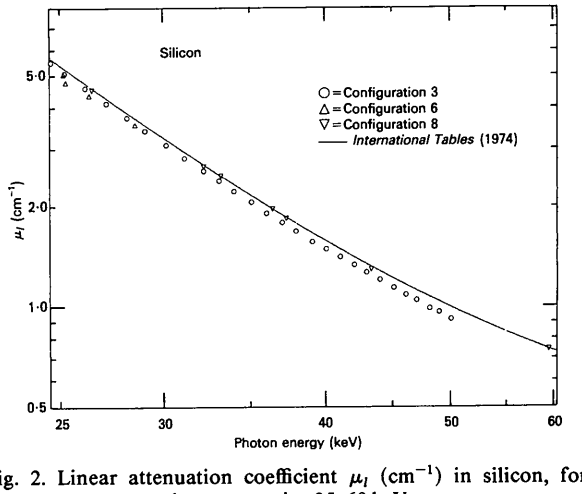


Fig. 2. Linear attenuation coefficient $\mu_l$ ($cm^{-1}$) in silicon, for photon energies 25–60 keV.

### 4.2. *Data taken using a Bremsstrahlung source*

Data taken for $\mu_l$ for the energy range 25 to 60 keV are plotted in Fig. 2. In this graph $\ln \mu_l$ is plotted as a function of $\ln E$. If photoelectric absorption is the dominant attenuation mechanism such a plot yields a straight line. The curvature of the plot in Fig. 2 for photon energies greater than 35 keV indicates that the other scattering processes become important for these photon energies. Two sets of data were taken using configuration 3 and these are in excellent agreement with one another.

Two data sets taken using no. 8, one of these a data point at 59·5 keV, are also plotted. Although the no. 8 data points appear to be systematically higher, by 3 to 5%, than measurements using no. 3 (also than some no. 6 measurements shown here), we consider the general agreement between data sets to be reasonable, given the differences in the experimental configurations. The curve plotted in Fig. 2 is fitted to the data derived from McMaster *et al.* (1969, 1970).

## 5. Discussion

In the previous section a comparison was made of the various techniques for the measurement of $\mu_l$ and some conclusions were drawn concerning the values to be chosen as the best measurements for silicon at a particular wavelength. Here we shall compare these values with those expected from theory.

There are two different approaches for combining the various photon–atom interaction contributions to the attenuation coefficient. In the first it is assumed that the photons interact with the material as though each atom in the material is unaffected by its neighbors and the total linear attenuation coefficient is given by the expression

$$\mu_l^+ = \mu_{pe} + \mu_C + \mu_R \qquad (15)$$

where $\mu_{pe}$, $\mu_C$ and $\mu_R$ are the photoelectric absorption and the Compton and Rayleigh scattering coefficients, respectively.

The second approach assumes that the assemblage of atoms behaves as though it were a large perfect single crystal for which cooperative Rayleigh scattering (Laue–Bragg scattering) and thermal diffuse scattering take place. Calculation of the Laue–Bragg scattering is a complicated process in general since it is extremely sensitive to crystal orientation and beam divergence. However, it is possible to choose the beam divergence and specimen orientation in such a manner as to minimize the number of lattice planes giving rise to Laue-Bragg scattering. In such a case the coherent scattering is reduced to the thermal diffuse scattering and

$$\mu_l^* = \mu_{pe} + \mu_C + \mu_{TD} \qquad (16)$$

where $\mu_{pe}$, $\mu_C$ and $\mu_{TD}$ are the photoelectric,

Table 2. *Calculated photon interaction contributions in silicon*

| Photon energy (keV) | Line | $\mu_i$ for Compton ($cm^{-1}$) | Rayleigh ($cm^{-1}$) | TDS ($cm^{-1}$) | photoelectric ($cm^{-1}$) |
|---|---|---|---|---|---|
| 8·048 | Cu $K\alpha_1$ | 0·222 | 1·861 | 0·213 | 143·3 |
| 8·907 | Cu $K\beta$ | 0·235 | 1·664 | 0·216 | 107·0 |
| 17·478 | Mo $K\alpha_1$ | 0·315 | 0·668 | 0·156 | 14·2 |
| 19·663 | Mo $K\beta$ | 0·325 | 0·560 | 0·1425 | 9·8 |
| 22·162 | Ag $K\alpha_1$ | 0·334 | 0·467 | 0·097 | 6·8 |
| 24·986 | Ag $K\beta$ | 0·342 | 0·389 | 0·068 | 4·72 |
| 40·06 | * | 0·357 | 0·183 | 0·044 | 1·072 |
| 59·5 | † | 0·356 | 0·0925 | 0·028 | 0·303 |

From Cromer & Liberman (1970) 8·048–22·162 keV; from Scofield (1973) with HFS corrections applied by Hubbell (1982) 24·986–59·5 keV.
* Line from *Bremsstrahlung.*
† Line from $^{241}$Am.

Table 3. *Comparison of experimental and theoretical linear attenuation coefficients in silicon, for photon energies* 8·048 *to* 59·57 keV

Also included are the values from *International Tables for X-ray Crystallography* (1974) (IT IV), allowing for the existence of thermal diffuse rather than Rayleigh scattering processes.

| Photon energy (keV) | Line | Theoretical values for $\mu_l$ ($cm^{-1}$) $\mu_l^+$ | $\mu_l^*$ | IT IV $\mu_l'$ | Experimental value for $\mu_l$ ($cm^{-1}$) |
|---|---|---|---|---|---|
| 8·048 | Cu $K\alpha_1$ | 145·3 | 143·7 | 150·0 | 144·6 (6)† |
| 8·907 | Cu $K\beta$ | 108·2 | 106·9 | 113·0 | 107·5 (6) |
| 17·478 | Mo $K\alpha_1$ | 15·19 | 14·68 | 14·7 | 14·60 (2) |
| 19·663 | Mo $K\beta$ | 10·834 | 10·40 | 10·34 | 10·38 (4) |
| 22·162 | Ag $K\alpha_1$ | 7·57 | 7·19 | 7·18 | 7·18 (2) |
| 24·986 | Ag $K\beta$ | 5·45 | 5·179 | 5·13 | 5·18 (4) |
| 40·06 | ‡ | 1·691 | 1·548 | 1·431 | 1·470 (2) |
| 59·5 | § | 0·901 | 0·832 | 0·675 | 0·742 (1) |

† The values given in parentheses are the errors in the final decimal place shown: 144·6 (6) ≡ 144·6 ± 0·6.

$$\mu_l^+ = \mu_{pe} + \mu_C + \mu_R,\ \mu_l^* = \mu_{pe} + \mu_C + \mu_{TD},\ \mu_l' = \mu_4 - \mu_R + \mu_{TD}.$$

‡ Line from *Bremsstrahlung.*
§ Line from $^{241}$Am.

Compton, and thermal diffuse components to the linear attenuation coefficients.

In Table 2, values derived from Cromer & Liberman's (1970) tables are listed. For the Compton-scattering component $\mu_C$, tabulations by different authors give substantially the same values as those derived from Hubbell *et al.* (1975) which are listed in Table 2. The Rayleigh scattering component $\mu_R$ found by interpolation to the data listed in Hubbell & Øverbø (1979) is also shown for those wavelengths of major interest to crystallographers. The thermal diffuse scattering contribution $\mu_{TD}$ has been calculated using the technique outlined in § 2.4.3.

The theoretical value of $\mu_l$ can now be presented according to which approach is taken: individual atom ($\mu_l^+$) or single crystal without Laue–Bragg scatter ($\mu_l^*$). Table 3 lists $\mu_l^+$ and $\mu_l^*$ and compares these with what are considered to be the best experimentally determined values for $\mu_l$. Also shown in Table 3 is the value of $\mu_l' = \mu_4 - \mu_R + \mu_{TD}$, where $\mu_4$ is the value listed in, or interpolated from, Hubbell, McMaster, Del Grande & Mallett (1974). This table uses calculated values of the Rayleigh scattered attenuation coefficient $\mu_R$. The values listed here show the Hubbell *et al.* (1974) values corrected to allow for thermal diffuse rather than Rayleigh scattering. Note the significant systematic difference between the experimental and the tabulated data set. It appears that a systematic error exists in the value of $\mu_{pe}$. In general, single-crystal rather than single-atom scattering seems to be the norm.

Further, significant discrepancies between theory and experiment occur only for those photon energies for which the Compton and thermal diffuse scattering cross sections are comparable with the photoelectric scattering cross section.

## 6. Concluding remarks

It is clear from the analysis of the data set out in Table 1 that one technique (no. 3) gives the most reliable results for the range of photon energies from 4 to 50 keV. For photon energies less than 4 keV configuration 6 can be used, whilst for energies higher than 50 keV configuration 3 is the only technique which can be used.

To ensure reliable results, however, it is necessary to consider the nature of the sample under investigation before deciding what measurement strategy to employ. The structure of the sample will dictate what collimation, monochromatization, detection and counting strategies are to be employed.

Furthermore, measurements of such important parameters as density, area and thickness should be made by the experimenter. Recourse to published values of density may lead to erroneous $\mu_l$ values being derived from correct $\mu_m$ values. Comparison of the measured and published values of density may give important information as to the homogeneity and impurity of the specimen.

It is also important to mount the sample normal to the beam and to vary the sample thickness to verify that the Beer–Lambert law is satisfied and a unique value of $\mu_l$ exists.

There is no clear evidence to establish which of the three theoretical tables for the photoelectric absorption cross section is to be preferred for the silicon specimens used in this study, and recalculations of the Compton scattering cross section do not yield values at variance with the computations of Hubbell *et al.* (1975). However, it must be remembered that the Compton-scattering profile of ensembles of atoms may differ from those of single atoms. See, for example, Cooper (1985).

In addition, the Rayleigh scattering cross sections contained in Hubbell & Øverbø (1979) are not inconsistent with the present results. However, for higher

photon energies, Rayleigh scattering cross sections based on the relativistic Hartree-Fock-Slater modified form factors of Schaupp *et al.* (1983) are expected to be more accurate.

Some doubt exists as to the accuracy of the calculations of the thermal diffuse scattering sections. For photon energies below 25 keV the effect of uncertainties in $\sigma_{TD}$ is not of much significance. However, above 25 keV inaccuracies in this compilation are significant, since the contribution to the total cross section of $\sigma_{TD}$ is significant in this energy regime.

Furthermore, the measurements of X-ray attenuation coefficients have been made at photon energies remote from the absorption edge of silicon. It is well known that within some hundreds of electron volts of an absorption edge oscillations occur in the X-ray attenuation coefficients: extended X-ray absorption fine structure (EXAFS) occurs. These arise because of interaction of the ejected photoelectron with atoms which surround the excited atom. It is no longer possible to consider the photoelectric absorption to be a single-atom process.

Thus care must be taken at all times to ensure that, whenever theoretical cross sections are being calculated, appropriate recognition is given to the effect of arrangement of atoms in the sample material.

The authors are greatly indebted to all the Project participants (listed in the Appendix) who have submitted their experimental results for inclusion in this paper, and in particular to Dr L. Gerward for his generous support and critical comments on this text.

One of us (DCC) also acknowledges the assistance of the Australian Research Grants Scheme, who provided some of the funds required to mount the project. The other (JHH) acknowledges support from the National Bureau of Standards Office of Standard Reference Data.

Technical assistance was provided by Mr Ken Dixon who machined the moulds for the specimen mounts and Mr Steve Downing who constructed the energy-dispersive double-crystal spectrometer system used to collect data for this project.

## APPENDIX

### Participants who have provided data used in this paper

CHAUDHURI, N. Department of Physics, University of North Bengal - PO Dt. Darjeeling, West Bengal, India PIN-734430.

CREAGH, D. C. Department of Physics, Royal Military College, Duntroon, ACT 2600, Australia.

DEL GRANDE, N. K. Lawrence Livermore National Laboratory, PO Box 808, Livermore, California 94550, USA.

GERWARD, L. Laboratory of Applied Physics III, Technical University of Denmark, Building 307, DK-2800 Lyngby, Denmark.

HARRIS, L. S. AND MCCUAIG, N. Department of Physics, University of Surrey, Guildford, Surrey GU2 5XH, England.

KODRE, A., HRIBAR, M. AND AJLEC, B. Department of Physics, J. Stefan Institute, University of E. Kardelj, YU-61001 Ljubljana, Yugoslavia.

LAWRENCE, J. L. Department of Physics, University of St. Andrews, North Haugh, St. Andrews, KY16 9SS, Scotland.

MEHROTRA, B. N. School of Physics, Universiti Sains Malaysia, Minden, Penang, Malaysia.

MIKA, J. F. AND MARTIN, L. J. Australian Radiation Laboratory, Lower Plenty Road, Yallambie, Victoria 3085, Australia.

NORRISH, K., HANCOCK, G. AND ROGERS, P. CSIRO Division of Soils, Urrbrae, Adelaide, South Australia.

O'CONNOR, B. School of Physics and Geosciences, WA Institute of Technology, Kent Street, Bentley, WA 6102, Australia.

UNO, R. Department of Physics, College of Humanities and Sciences, 3-25-40 Sakurajosni Setagaya-Ku, Tokyo, Japan.

### References

ALLEN, S. J. M. (1935). *X-rays in Theory and Experiment*, edited by A. H. COMPTON & S. K. ALLISON, pp. 799-806. New York: Van Nostrand.

ALLEN, S. J. M. (1969). *Handbook of Chemistry and Physics*, edited by R. C. WEAST, pp. E-143-E-144. Cleveland: The Chemical Rubber Co.

BAND, I. M., KHARITONOV, YU. I. & TRZHASKOVSKAYA, M. B. (1979). *At. Data Nucl. Data Tables*, **23**, 443-505.

BARKLA, C. G. & SADLER, C. A. (1907). *Philos. Mag.* **14**, 408-422.

BEARDEN, J. A. & BURR, A. F. (1967). *Rev. Mod. Phys.* **39**, 125-142.

BERTIN, E. P. (1975). *Principles and Practice of X-ray Spectrometric Analysis*, 2nd ed., pp. 219-415. New York: Plenum.

BRYSK, H. & ZERBY, C. D. (1968). *Phys. Rev.* **171**, 292-298.

CHIPMAN, D. R. (1969). *Acta Cryst.* A**25**, 209-214.

COOPER, M. J. (1985). *Rep. Prog. Phys.* **48**, 415-477.

CREAGH, D. C. (1976). *J. Phys. E*, **9**, 88-90.

CREAGH, D. C. (1978). *Adv. X-ray Anal.* **21**, 149-153.

CROMER, D. T. (1969). *J. Chem. Phys.* **50**, 4857-4859.

CROMER, D. T. & LIBERMAN, D. (1970). *J. Chem. Phys.* **53**, 1891-1898.

CROMER, D. T. & MANN, J. B. (1967). *J. Chem. Phys.* **47**, 1892-1893.

CROMER, D. T. & WABER, J. T. (1965). *Acta Cryst.* **18**, 104-109.

DESLATTES, R. D. (1969). *Acta Cryst.* A**25**, 89-93.

GERWARD, L. (1981). *J. Phys. B*, **14**, 3389-3395.

GERWARD, L. (1982). *High-Precision X-ray Attenuation Coefficients Measured by an Energy-Dispersive Method. Revised Values for Silicon, Copper and Graphite.* LTF III Report No. 40. Tech. Univ. of Denmark, Lyngby, Denmark.

GERWARD, L., THUESEN, G., STIBIUS JENSEN, M. & ALSTRUP, I. (1979). *Acta Cryst.* A**35**, 852-857.

HEINRICH, K. F. J. (1966). *The Electron Microprobe*, edited by T. D. MCKINLEY, K. F. J. HEINRICH & D. B. WITTRY, pp. 296-377. New York: John Wiley & Sons.

HENINS, I. (1964). *J. Res. Natl Bur. Stand. Sect. A*, **68**, 529-533.

HENKE, B. L., LEE, P., TANAKA, T. J., SHIMABUKURO, R. L. & FUJIKAWA, B. K. (1982). *At. Data Nucl. Data Tables*, **27**, 1-144.

HILDEBRANDT, G., STEPHENSON, J. D. & WAGENFELD, H. (1973). *Z. Naturforsch. Teil A*, **28**, 588-600.

HILDEBRANDT, G., STEPHENSON, J. D. & WAGENFELD, H. (1975). *Z. Naturforsch. Teil A*, **30**, 697-707.
HUBBELL, J. H. (1969). *Photon Cross Sections, Attenuation Coefficients, and Energy Absorption Coefficients from* 10 keV *to* 100 GeV. Report NSRDS-NBS 29. Gaithersburg: National Bureau of Standards.
HUBBELL, J. H. (1971). *At. Data*, **3**, 241-297.
HUBBELL, J. H. (1982). *Int. J. Appl. Radiat. Isot.* **33**, 1269-1290.
HUBBELL, J. H., MCMASTER, W. H., DEL GRANDE, N. K. & MALLETT, J. H. (1974). *International Tables for X-ray Crystallography*, Vol. IV, pp. 47-70. Birmingham: Kynoch Press. (Present distributor D. Reidel, Dordrecht.)
HUBBELL, J. H. & ØVERBØ, I. (1979). *J. Phys. Chem. Ref. Data*, **8**, 69-105.
HUBBELL, J. H., VEIGELE, W. J., BRIGGS, E. A., BROWN, R. T., CROMER, D. T. & HOWERTON, R. J. (1975). *J. Phys. Chem. Ref. Data*, **4**, 471-538; erratum: *J. Phys. Chem. Ref. Data* (1977). **6**, 615-616.
*International Tables for X-ray Crystallography* (1974). Vol. IV. Birmingham: Kynoch Press. (Present distributor D. Reidel, Dordrecht.)
JACKSON, D. F. & HAWKES, D. J. (1981). *Phys. Rep.* **70**, 169-233.
KIRBY, R. K., HAHN, T. A. & ROTHROCK, B. D. (1972). *American Institute of Physics Handbook*, 3rd ed., p. 4-129. New York: McGraw-Hill.
KLUG, H. P. & ALEXANDER, L. E. (1973). *X-ray Diffraction Procedures*, 2nd ed., pp. 271-417. New York: John Wiley & Sons.
KOCH, B., MACGILLAVRY, C. H. & MILLEDGE, H. J. (1962). *International Tables for X-ray Crystallography*, Vol. III, pp. 157-192. Birmingham: Kynoch Press. (Present distributor D. Reidel, Dordrecht.)
LANG, A. R. (1958). *J. Appl. Phys.* **29**, 597-598.
LAWRENCE, J. L. (1977). *Acta Cryst.* A**33**, 343.
LEROUX, J. & THINH, T. P. (1977). *Revised Tables of X-ray Mass Attenuation Coefficients*. Quebec: Corporation Scientifique Claisse, Inc.
LIEBHAFSKY, H. A., PFEIFFER, H. G., WINSLOW, E. H. & ZEMANY, P. D. (1960). *X-ray Absorption and Emission in Analytical Chemistry*, pp. 313-317. New York: John Wiley & Sons.
MCMASTER, W. H., DEL GRANDE, N. K., MALLETT, J. H. & HUBBELL, J. H. (1969, 1970). *Compilation of X-ray Cross Sections*. Report UCRL-50174. (Section I, 1970; Section II, 1969; Section III, 1969; Section IV, 1969). Lawrence Livermore National Laboratory, Livermore, California.
MARCO, J. J. DE & SUORTTI, P. (1971). *Phys. Rev. B*, **4**, 1028-1033.
MIKA, J. F., MARTIN, L. J. & BARNEA, Z. (1985). *J. Phys. C*, **18**, 5215-5223.
MONTENEGRO, E. C., BAPTISTA, G. B. & DUARTE, P. W. E. P. (1978). *At. Data Nucl. Data Tables*, **22**, 131-177.
NORDFORS, B. (1960). *Ark. Fys.* **18**, 37-47.
PLECHATY, E. F., CULLEN, E. E. & HOWERTON, R. J. (1981). *Tables and Graphs of Photon-Interaction Cross-Sections from* 0·1 keV *to* 100 MeV *Derived from the LLL Evaluated-Nuclear-Data Library*. Report UCRL-50400, Vol. 6, Rev. 3. Lawrence Livermore National Laboratory, Livermore, California.
RÖNTGEN, W. C. (1895). *Sitzungsber. Würzburger Physik.-Medic. Gesellschaft.*
SANO, H., OHTAKA, K. & OHTSUKI, Y. H. (1969). *J. Phys. Soc. Jpn*, **27**, 1254-1261.
SCHAUPP, D., SCHUMACHER, M., SMEND, F., RULLHUSEN, P. & HUBBELL, J. H. (1983). *J. Phys. Chem. Ref. Data*, **12**, 467-512.
SCOFIELD, J. H. (1973). *Theoretical Photoionization Cross Sections from* 1 *to* 1500 keV. Report UCRL-51326. Lawrence Livermore National Laboratory, Livermore, California.
STORM, E. & ISRAEL, H. I. (1970). *Nucl. Data Tables*, A**7**, 565-681.
THEISEN, R. & VOLLATH, D. (1967). *Tables of X-ray Mass Attenuation Coefficients*. Düsseldorf: Verlag Stahleisen.
VEIGELE, W. J. (1973). *At. Data*, **5**, 51-111.
VICTOREEN, J. A. (1949). *J. Appl. Phys.* **20**, 1141-1147.

*Acta Cryst.* (1987). A**43**, 112-117

# Maximum Entropy Solution of a Small Centrosymmetric Crystal Structure

BY S. F. GULL, A. K. LIVESEY* AND D. S. SIVIA

*Cavendish Laboratory, University of Cambridge, Madingley Road, Cambridge CB3 0HE, England*

(*Received* 27 *February* 1986; *accepted* 22 *July* 1986)

## Abstract

The maximum entropy (MAXENT) method has been used *ab initio* to solve a previously determined small centrosymmetric crystal structure, bis(acetylacetonato)dichlorotin, $C_{10}H_{14}Cl_7O_4Sn$ [Miller & Schlemper (1978). *Inorg. Chim. Acta*, **30**, 131-134; Webster & Wood (1981). *J. Chem. Res.* (*M*), pp. 0450-0456]. The resulting electron density maps are of a very high quality, comparable or even superior to the conventional maps calculated from the refined phases. The method, therefore, holds good promise for the solution of larger and more difficult structures. The addition of simple chemical and symmetry information about the heavy atoms in the structure greatly improves the reconstruction and shows the capability of MAXENT to solve structures from partial fragments.

## 1. Introduction

Although the theory of solving the phaseless Fourier transform problem by means of the maximum entropy (MAXENT) method has been extensively discussed (Collins, 1982; Steenstrup & Wilkins, 1984; Bricogne, 1984; Livesey & Skilling, 1985; Navassa, 1985; and

* Present address: Department of Applied Mathematics and Theoretical Physics, Silver Street, Cambridge, and Medical Research Council, Hills Road, Cambridge.

0108-7673/87/010112-06$01.50 